COMPUTER METHODS IN BIOMECHANICS AND BIOMEDICAL ENGINEERING, 2015
http://dx.doi.org/10.1080/10255842.2015.1105965

Taylor & Francis
Taylor & Francis Group

Computational modeling of acute myocardial infarction

P. Sáez[a,1] and E. Kuhl[b]

[a]Mathematical Institute, University of Oxford, Oxford, UK; [b]Department of Mechanical Engineering, Stanford University, Stanford, CA, USA

ABSTRACT

Myocardial infarction, commonly known as heart attack, is caused by reduced blood supply and damages the heart muscle because of a lack of oxygen. Myocardial infarction initiates a cascade of biochemical and mechanical events. In the early stages, cardiomyocytes death, wall thinning, collagen degradation, and ventricular dilation are the immediate consequences of myocardial infarction. In the later stages, collagenous scar formation in the infarcted zone and hypertrophy of the non-infarcted zone are auto-regulatory mechanisms to partly correct for these events. Here we propose a computational model for the short-term adaptation after myocardial infarction using the continuum theory of multiplicative growth. Our model captures the effects of cell death initiating wall thinning, and collagen degradation initiating ventricular dilation. Our simulations agree well with clinical observations in early myocardial infarction. They represent a first step toward simulating the progression of myocardial infarction with the ultimate goal to predict the propensity toward heart failure as a function of infarct intensity, location, and size.

ARTICLE HISTORY
Received 7 December 2014
Accepted 6 October 2015

KEYWORDS
Biomechanics; growth; smooth muscle cells; hypertension; finite element method

1. Introduction

Heart disease is the number one cause of death worldwide. This high death rate has lead to intense research in many fields of biology and engineering. Treatment of myocardial infarction has been evolving rapidly with the understanding of the mechanisms underpinning its progression. There is a clear correlation between infarct size and ejection fraction. Therefore, many clinical therapies have been devoted to maintain normal ejection fractions mechanically, pharmacologically, interventionally, and surgically (Cheng et al. 2006; Tiyyagura & Pinney 2006; Passier et al. 2008).

Cardiac tissue is composed of two major components that determine its mechanical behavior, cardiac cells – primarily cardiomyocytes, and extracellular matrix – primarily collagen. Cardiomyocytes are terminally differentiated from myoblasts. They comprise approximately 25% of all cells in the heart and, in their healthy state, they exert tension by contraction to pump blood to the rest of the body. Cardiomyocytes contraction is tightly regulated by ion concentrations inside and outside the cell. Their action potential is a result of sodium, potassium, and calcium concentration differences across the cell membrane.

The extracellular matrix provides a scaffold-type structure that provides the mechanical strength. Collagen I and III are the most important types of collagen in the extracellular matrix and the amount and distribution of the collagen fibers critically influence cardiac performance. Collagen I and III are synthesized mainly by myofibroblasts. Collagen I, which is associated with thick fibers, constitutes 85% of all the collagen in the heart; collagen III is associated with thin fibers. Collagen degradation and deposition is mainly influence by growth factors including TGF-β (Border & Noble 1994) and the MMP/TIMP ratio (Visse & Nagase 2003).

The healthy heart is conditioned by a continuous supply of oxygen and a balance between nutrient supply and demand. Myocardial infarction occurs when blood supply is interrupted and nutrient supply is compromised. During myocardial infarction, blood supply is interrupted by plaque formation in the coronary arteries (Fuster 1994) and the infarcted myocardium loses its contractile features. If the damaged region is large enough, myocardial infarction will trigger chronic heart failure. With an increasing tissue, hypoxia Adenosine Triphosphate (ATP) depletes, which causes failure of cardiac contraction. Two main types of cell deaths have been observed in hypertensive cardiomyopathy (González et al. 2003) and in ischemic heart disease (Buja et al. 1993): oncosis and apoptosis (Kanduc et al. 2002). Oncosis results in cell swelling and is associated with ischemic damage.

CONTACT P. Sáez saez@maths.ox.ac.uk
[1]Applied Mechanics and Bioengineering, Aragon Institute of Engineering Research, University of Zaragoza, Zaragoza, Spain.

Oncosis is the dominating process in the later stages, from 4 to 12 days after myocardial infarction. Apoptosis is an energy-related, ATP-dependent process. Apoptosis is associated with cell shrinkage and programmed cell death (MacLellan & Schneider 1997; González et al. 2003). Apoptosis is involved in early stages of cell death, 4-8 hours after infarction, on ischemic injury and during reperfusion.

Morphological and mechanical changes in the heart after myocardial ischemia follow a well-defined pattern in time (Blankesteijn et al. 2001; Jugdutt 2003). Similar to wound healing (Buganza Tepole & Kuhl 2003), post-infarction remodeling has a short and a long timescale and establishes a threshold 72 hours post infarction (Sutton & Sharpe 2000). The first stage, cardiomyocyte death, initiates a cascade of biochemical signaling processes in the form of inflammatory reactions in the infarct zone. Cell death and collagen degradation trigger wall thinning. Besides reducing structural support, this process enable cell migration into the infarcted region and neutrophils release matrix metalloproteinase into the infarct zone (Cleutjens et al. 1995). Collagen degradation begin 30 min post-infarction and continues throughout the entire first week (Knowlton & Chien 1999; Etoh et al. 2001). Collagen degradation is a rather local process: it is observed only in the infarcted region, not in the surrounding tissue.

In the short term, the most important morphological and mechanical consequence is wall thinning, associated with collagen degradation and expansion of the ventricle. Figure 1 displays the immediate consequences of myocardial infarction: Cardiomyocyte death and collagen degradation. Within hours, the reduction of extracellular matrix can lead to ventricular expansion (Erlebacher et al. 1984), which can eventually result in wall rupture (Eaton et al. 1979). The digestion of intercellular collagen fibers promotes the slippage of dead myofilaments that cause expansion of the infarct zone (Olivetti et al. 1990). This expansion of the ventricles alters the stroke volume. To preserve the stroke volume and optimize function in the sense of the Frank-Starling curves, a number of mechanical processes take place in the infarct region, the border zone, and the healthy myocardium.

In the long term, myofibroblast invades the infarct zone. Myofibroblasts acquire contractile properties that promote wound contraction. At the same time, the formation of new collagen begins to compensate cardiac expansion and stabilize the infarcted heart (Ertl & Frantz 2005).

In the following sections, we will address these molecular processes in view of a systems biology-based approach and their mechanical consequences (Buganza Tepole & Kuhl xxxx). Although important efforts have been made toward simulating infarct-induced remodeling processes in the heart (Goktepe, Abilez, & Kuhl 2010; Lee, Wall, et al. 2014), the multiscale coupling between molecular events and organ function has received little attention to date. In the first section, we will discuss a simple model of cardiomyocyte death, which will serve as a trigger variable for subsequent processes. This will allow us to model ventricular wall thinning in response to myocardial infarction. We explore collagen degradation and characterize its impact on ventricular expansion. Finally, we suggest a computational mechanics model of the heart for the different stages of cardiac adaptation and we compare the results with observations reported in the literature.

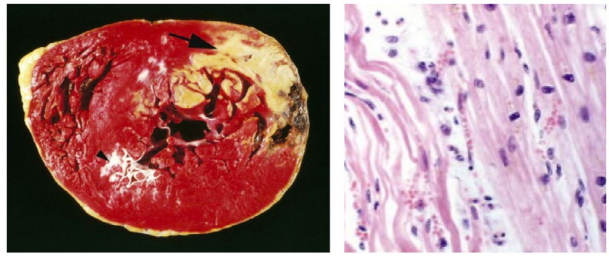

Figure 1. Acute myocardial infarction at the macroscopic and microscopic scales. Histochemical staining reveals cardiomyocyte death in the posterolateral left ventricle, left. Histopathologic changes manifest themselves in wavy fibers at the periphery of the infarct, left, compared to the normal fibers in the healthy myocardium, right. The widened spaces between the dead fibers contain edema fluid and facilitate cardiomyocyte slippage, right. Adopted with permission from Kumar et al. (2014).

2. Methods: model problem of infarcted heart

Myocardial ischemia is characterized by a decreased blood supply. Figure 2 illustrates myocardial infarction as a result of plaque formation in the coronary arteries. Let us recall the basic kinematics of finite deformation. The deformation gradient $\mathbf{F} = \nabla_X \boldsymbol{\varphi}$, tangent to the motion $\boldsymbol{\varphi}$, represents a two-point linear map over the reference configuration. Within the framework of finite growth, the key kinematic assumption is the multiplicative decomposition of the deformation gradient $\mathbf{F}$ into an elastic part $\mathbf{F}^{\mathrm{e}}$ and a growth part $\mathbf{F}^{\mathrm{g}}$ (Rodriguez et al. 1994),

$$\mathbf{F} = \nabla_X \boldsymbol{\varphi} = \mathbf{F}^{\mathrm{e}} \cdot \mathbf{F}^{\mathrm{g}}. \tag{1}$$

The underlying concept follows the multiplicative decomposition in finite elastoplasticity (Lee 1969). We can think of the growth tensor $\mathbf{F}^{\mathrm{g}}$ as a second-order internal variable to characterize arbitrary forms of isotropic or anisotropic growth (Menzel & Kuhl 2012). Here we consider two types of growth and parameterize the two growth tensors exclusively in terms of two single scalar-valued internal variables, the growth multipliers $\vartheta^{\perp}$ and $\vartheta^{\parallel}$, which characterize growth in the muscle sheet direction $\mathbf{n}^{\perp}$ and in the muscle fiber direction $\mathbf{n}^{\parallel}$ (Goktepe, Abilez, & Kuhl

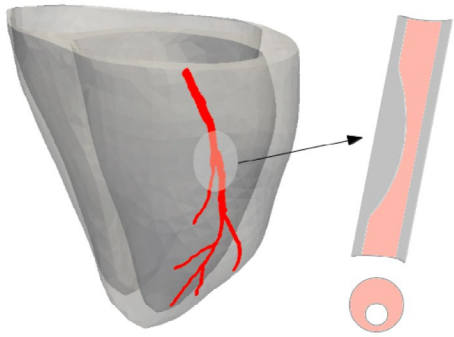

Figure 2. Schematic drawing of the left anterior coronary artery and the obstruction of blood flow in the detailed view during myocardial infarction.

2010; Sáez et al. 2014). The Jacobian of the deformation gradient $J = \det(\mathbf{F})$ characterizes changes in volume, which we can decompose into reversible elastic volume changes $J^e = \det(\mathbf{F}^e)$ and volume changes attributed to growth, $J^g = \det(\mathbf{F}^g)$,

$$J = \det(\mathbf{F}) = J^e\, J^g. \tag{2}$$

We further introduce the right Cauchy Green tensor,

$$\mathbf{C} = \mathbf{F}^t \cdot \mathbf{F} = (\mathbf{F}^g)^t \cdot \mathbf{C}^e \cdot \mathbf{F}^g \quad \text{with} \quad \mathbf{C}^e = (\mathbf{F}^e)^t \cdot \mathbf{F}^e, \tag{3}$$

as the covariant pull back of the elastic right Cauchy Green tensor $\mathbf{C}^e$. It remains to specify the mechanisms of growth and with them the kinematics and kinetics of the growth tensor $\mathbf{F}^g$.

2.1. Cardiomyocyte death and ventricular wall thinning

Diminished oxygen supply causes cell death via necrosis or apoptosis. We model cell death by means of diffusion phenomena originating from several locations across the heart wall. These points represent ramifications of the left anterior descending coronary artery into arterioles. We characterize the reduction in the oxygen concentration of the cardiomyocytes as a result of impaired blood supply as

$$\dot{c}_{O_2} = \mathrm{Div}\,(\mathbf{q}_{O_2}) + \mathcal{Q}_{O_2}, \tag{4}$$

where c_{O_2} is the normalized oxygen concentration, $\mathbf{q}_{O_2} = -D_{O_2}\,\nabla c_{O_2}$ is the diffusion of oxygen in the myocardial tissue and $\mathcal{Q}_{O_2}$ is the oxygen source. For the particular problem of the ventricular wall thinning, we define the growth tensor as

$$\mathbf{F}^g = \mathbf{I} + [\,\vartheta^\perp - 1\,]\,\mathbf{n}^\perp \otimes \mathbf{n}^\perp, \tag{5}$$

where $\vartheta^\perp$ is the scalar-valued growth multiplier that defines the amount of growth or shrinkage along the sheet vector $\mathbf{n}^\perp$ (Goktepe, Abilez, & Kuhl 2010; Rausch et al. 2011). With the sheet vector pointing radially outward,

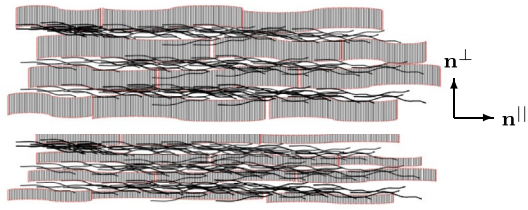

Figure 3. Healthy and infarcted myocardium. Loss of oxygen causes cardiomyocyte death, which results in a loss of volume and ventricular wall thinning modeled through negative growth in the thickness direction $\mathbf{n}^\perp$.

positive growth, $\vartheta^\perp > 1$, results in a thickening of the myocardial wall, while negative growth, $\vartheta^\perp < 1$, results in wall thinning (Goktepe, Abilez, Parker, et al. 2010). The function $\phi(c_{O_2}) = c_{O_2} - 1$ represents the growth criterion. We define the evolution of the growth multiplier $\vartheta^\perp$ it in terms of an oxygen concentration function $\phi(c_{O_2})$, and a threshold function $\kappa(\vartheta^\perp)$ for $\phi(c_{O_2}) < 0$,

$$\dot{\vartheta}^\perp = \kappa(\vartheta^\perp)\,\phi(c_{O_2}), \tag{6}$$

where
$\vartheta^\perp_{\min}$ sets a growth threshold while τ and γ control the evolution of the growth process (Himpel et al. 2005).

$$\kappa(\vartheta^\perp) = \frac{1}{\tau}\left[\frac{\vartheta^\perp - \vartheta^\perp_{\min}}{1 - \vartheta^\perp_{\min}}\right]^\gamma. \tag{7}$$

Unlike previous mechanically driven growth, our model is oxygen-driven, which is not a mechanical property. Figure 3 illustrates the mechanism by which wall thinning occurs: Due to a reduction in oxygen supply, cell death is initiated and results in a loss of volume. This volume loss manifests itself in negative cardiomyocyte growth and ventricular wall thinning.

2.2. Collagen degradation and ventricular dilation

During the early stages of the remodeling process, dysfunctional cardiomyocytes release matrix metalloproteinase, which causes increased collagen degradation. We model changes in matrix metalloproteinase, c_{MMP}, through the following rate equation (Sáez et al. 2013),

$$\dot{c}_{MMP} = \mathcal{Q}_{MMP} \;\text{ with }\; \mathcal{Q}_{MMP} = \left[\frac{c_{MMP}}{c^*_{MMP}}\right]^{-m} [\,1 - c_{O_2}\,], \tag{8}$$

where c_{O_2} is the normalized oxygen concentration, c_{MMP} is the density of matrix metalloproteinases, c^*_{MMP} is its initial value, and the exponent m controls its evolution. We assume that the collagen concentration c_{col} is correlated to the intensity of matrix metalloproteinase c_{MMP} through the scaling coefficient γ_{MMP},

$$\dot{c}_{\text{col}} = \gamma_{\text{MMP}}\, \dot{c}_{\text{MMP}}\,. \tag{9}$$

The continuing collagen turnover and increase in collagen degradation makes the ECM to lose its ability to serve as a scaffold of the cardiomyocytes. This degradation makes the ventricle to expand along time with the cardiac cycles. This process also softens the ventricular wall. We model ventricular dilation mathematically similar as wall thinning. We introduce the growth tensor $\mathbf{F}^{\text{g}}$ as

$$\mathbf{F}^{\text{g}} = \mathbf{I} + [\,\vartheta^{\parallel} - 1\,]\,\mathbf{n}^{\parallel} \otimes \mathbf{n}^{\parallel}, \tag{10}$$

where $\vartheta^{\parallel}$ is the scalar-valued growth multiplier that defines the amount of growth or shrinkage along the cardiomyocyte's long axis $\mathbf{n}^{\parallel}$ (Goktepe, Abilez, & Kuhl 2010). With the cardiomycyte vector pointing helically around the heart, positive growth, $\vartheta^{\parallel} > 1$, results in a dilation of the ventricles (Goktepe, Abilez, Parker, et al. 2010). Ventricular dilation is governed through the scalar-valued parameter $\vartheta^{\parallel}$. We model the evolution of ventricular dilation as

$$\dot{\vartheta}^{\parallel} = \kappa(\vartheta^{\parallel})\,\phi(c_{\text{col}}), \tag{11}$$

where the dilation function, $\phi(c_{\text{col}}) = 1 - c_{\text{col}}$, is parameterized in terms of the collagen concentration c_{col} and

$$\kappa(\vartheta^{\parallel}) = \frac{1}{\tau}\left[\frac{\vartheta^{\max} - \vartheta^{\parallel}}{\vartheta^{\max} - 1}\right]^{\gamma}, \tag{12}$$

for $\phi(c_{\text{col}}) > 0$, controls dilation through the threshold $\vartheta^{\max}$.

2.3. Mechanical model

Last, we define the mechanical problem and incorporate the characteristic features of quasi-incompressibility, non-linearity, and finite strains. We model quasi-incompressibility – mainly attributed to the water content – through the volumetric-isochoric decomposition of the deformation (Flory 1961). We decouple the elastic part of the deformation gradient $\mathbf{F}^{\text{e}}$ into dilatational and isochoric parts as

$$\mathbf{F}^{\text{e}} = (\,J^{\text{e}})^{1/3}\bar{\mathbf{F}}^{\text{e}} \quad \text{with} \quad J^{\text{e}} = \det(\mathbf{F}^{\text{e}}) \quad \text{and} \quad \bar{\mathbf{F}}^{\text{e}} = (\,J^{\text{e}})^{-1/3}\mathbf{F}^{\text{e}}. \tag{13}$$

We adopt a finite hyperelastic framework to capture the non-linear behavior and introduce the following strain energy density function (Holzapfel & Ogden 2009),

$$\begin{aligned}\Psi &= \Psi_{\text{vol}}(J^{\text{e}}) + \Psi_{\text{iso}}(\bar{I}_1^{\text{e}}, \bar{I}_4^{\text{e}}) \quad \text{with} \\ \Psi_{\text{iso}}(\bar{I}_1^{\text{e}}, \bar{I}_4^{\text{e}}) &= \Psi_1(\bar{I}_1^{\text{e}}) + \Psi_4(\bar{I}_4^{\text{e}}),\end{aligned} \tag{14}$$

where Ψ_{vol} is the volumetric part parameterized in terms of the elastic Jacobian J^{e}, and Ψ_{iso} is the isochoric part parameterized in terms of the first and forth invariants $\bar{I}_1^{\text{e}}$ and $\bar{I}_4^{\text{e}}$ of the isochoric elastic right Cauchy Green deformation tensor $\bar{\mathbf{C}}^{\text{e}}, = (\bar{\mathbf{F}}^{\text{e}})^{\text{t}} \cdot \bar{\mathbf{F}}^{\text{e}}$

$$\bar{I}_1^{\text{e}} = \bar{\mathbf{C}}^{\text{e}}{:}\mathbf{I} \quad \text{and} \quad \bar{I}_4^{\text{e}} = \bar{\mathbf{C}}^{\text{e}}{:}[\,\mathbf{n}^{\parallel} \otimes \mathbf{n}^{\parallel}\,]. \tag{15}$$

Here we have further decomposed the isochoric energy to independently characterize the isotropic and anisotropic response, $\Psi_{\text{iso}}(\bar{I}_1^{\text{e}}, \bar{I}_4^{\text{e}}) = \Psi_1(\bar{I}_1^{\text{e}}) + \Psi_4(\bar{I}_4^{\text{e}})$ For the isotropic contribution, we adopt an exponential form,

$$\Psi_1(\bar{I}_1^{\text{e}}) = \frac{a}{2b}\left[\,\exp(\,b[\bar{I}_1^{\text{e}} - 3]^2) - 1\right], \tag{16}$$

where a and b are material parameters. For the anisotropic contribution, we adopt the classical Holzapfel model (Holzapfel 2000),

$$\Psi_4(\bar{I}_4^{\text{e}}) = \frac{k_1}{2\,k_2}\left[\,\exp(\,k_2[\bar{I}_4^{\text{e}} - 1]^2) - 1\,\right] \tag{17}$$

with parameters $a = 0.5, b = 7.2, k_1 = 15.2$ and $k_2 = 20.5$ (Goktepe et al. 2011). The above decomposition of the strain energy density function naturally affects the elastic second Piola-Kirchhoff stress (Marsden & Hughes 1994; Holzapfel 2000),

$$\mathbf{S}^{\text{e}} = 2\,\partial_{\mathbf{C}^{\text{e}}}\Psi_{\text{vol}}(J^{\text{e}}) + 2\,\partial_{\mathbf{C}^{\text{e}}}\Psi_{\text{iso}}(\bar{I}_1^{\text{e}}, \bar{I}_4^{\text{e}}) = \mathbf{S}^{\text{e}}_{\text{vol}} + \mathbf{S}^{\text{e}}_{\text{iso}}, \tag{18}$$

which also consists of volumetric and an isochoric contributions,

$$\begin{aligned}\mathbf{S}^{\text{e}}_{\text{vol}} &= 2\,\partial_{\mathbf{C}^{\text{e}}}\Psi_{\text{vol}} \quad \text{and} \\ \mathbf{S}^{\text{e}}_{\text{iso}} &= 2\,\partial_{\bar{\mathbf{C}}^{\text{e}}}\Psi_{\text{iso}}{:}\partial_{\mathbf{C}^{\text{e}}}\bar{\mathbf{C}}^{\text{e}} = (\,J^{\text{e}})^{-2/3}\,\mathbb{P}^{\text{e}}{:}\bar{\mathbf{S}}^{\text{e}}.\end{aligned} \tag{19}$$

Here $\bar{\mathbf{S}}^{\text{e}} = \partial_{\bar{\mathbf{C}}^{\text{e}}}\Psi_{\text{iso}}(\bar{\mathbf{C}}^{\text{e}})$ is the fictitious second Piola-Kirchhoff stress $\mathbb{P}^{\text{e}} = \mathbb{I} - \frac{1}{3}\,(\mathbf{C}^{\text{e}})^{-1} \otimes \mathbf{C}^{\text{e}}$ is the fourth order projection tensor (Holzapfel 2000). The total second Piola-Kirchhoff stress

$$\mathbf{S} = 2\partial_{\mathbf{C}}\Psi = 2\partial_{\mathbf{C}^{\text{e}}}\Psi{:}\partial_{\mathbf{C}}\mathbf{C}^{\text{e}} = \mathbf{F}^{\text{g}-1} \cdot \mathbf{S}^{\text{e}} \cdot \mathbf{F}^{\text{g-t}}, \tag{20}$$

then follows from the contravariant pull back of the elastic second Piola-Kirchhoff stress $\mathbf{S}^{\text{e}}$ of Equation (18).

2.4. Numerical implementation

The diffusion problem is solved, with standard elements and pre-implemented constitutive equations, with the commercial software ABAQUS (Dassault Systemes Simulia Corp., Providence, RI, USA). In the mechanical part, we introduce the growth multipliers, $\vartheta^{\perp}$ for ventricular wall thinning and $\vartheta^{\parallel}$ for ventricular dilation, as internal variables on the integration point level. To solve

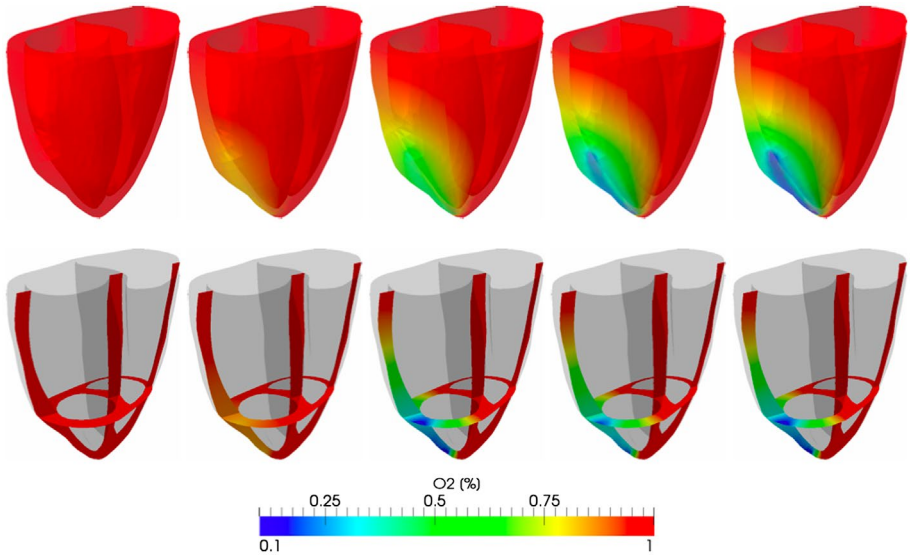

Figure 4. Evolution of oxygen supply as a trigger for cardiomyocyte death following left anterior descending arterial occlusion.

the growth kinetics in time, we adapt an implicit Euler backward scheme,

$$\dot{\vartheta} = [\vartheta - \vartheta^{n}]/\Delta t, \tag{21}$$

where $\Delta t = t - t^{n}$ Denotes the current time increment, with the understanding that we omit the superscript $(\circ)^{n+1}$ for ease of notation. To solve for the evolution of growth, we apply a local Newton iteration with the discrete local residual,

$$\mathcal{R} = \vartheta - \vartheta^{n} - \phi\, \kappa(\vartheta)\, \Delta t, \tag{22}$$

and its local tangent,

$$\mathcal{K} = \mathrm{d}_{\vartheta}\mathcal{R} = 1 - \phi\, \partial_{\vartheta}\kappa\, \Delta t. \tag{23}$$

For ventricular wall thinning, $\partial_{\vartheta}\kappa^{\perp} = \gamma\kappa^{\perp}/[\vartheta^{\perp} - \vartheta^{\perp}_{\min}]$; for ventricular dilation, $\partial_{\vartheta}\kappa^{\parallel} = -\gamma\kappa^{\parallel}/[\vartheta^{\parallel}_{\max} - \vartheta^{\parallel}]$. The incremental update of the growth multiplier takes the following format,

$$\vartheta \leftarrow \vartheta^{n} - \mathcal{R}/\mathcal{K}, \tag{24}$$

which we use to iterate until the absolute value of the residual reaches a user-defined threshold level. At local equilibrium, we store the growth multiplier $\vartheta^{\perp}$ or $\vartheta^{\parallel}$, and successively calculate the growth tensor $\boldsymbol{F}^{g}$ using Equation (5) or (10), calculate the elastic tensor $\mathbf{F}^{e}$ and its Jacobian J^{e} using Equation (1), calculate the isochoric elastic tensor $\bar{\mathbf{F}}^{e}$ using Equation (13), and calculate the isochoric elastic Cauchy Green deformation tensor $\bar{\mathbf{C}}^{e}$ along with its invariants $\bar{I}_1^{e}$ and $\bar{I}_4^{e}$ using Equation (15). Last, we calculate the elastic second Piola-Kirchhoff stress $\mathbf{S}^{e}$ using Equation (18) and the total second Piola-Kirchhoff stress $\mathbf{S}$ using Equation (20). To solve the set of finite element equations within a global Newton iteration, we finally calculate the fourth order tensor of tangent moduli $\mathbf{C} = 2\,\mathrm{d}_{\mathbf{C}}\mathbf{S}$, which relate increments in stress and strain and are essential for an efficient finite-element implementation.

3. Results

3.1. Cardiomyocyte death and wall thinning

Figure 4 illustrates the progression of cell death due to a 90% decrease in the blood supply from the left anterior descending coronary artery. As initial conditions, we reduce the local oxygen concentration in the affected ischemic area to $c_{O^2}(t_0) = 0.1$and assume that the remaining tissue is initially unaffected by the ischemic event with $c_{O^2}(t_0) = 1.0$. Figure 4 documents the gradual progression of the cell death in regions of reduced oxygen supply. Cell necrosis is a trigger for several processes that subsequently occur across the heart.

Figure 5 illustrates the resulting thinning of the left ventricular wall. Wall thinning naturally takes largest values in regions of largest cardiomyocyte death. The maximum relative reduction in the wall thickness occurred in the center of the infarct and was 23%.

3.2. Collagen degradation and ventricular dilation

Figure 6 shows the evolution of collagen degradation after partial occlusion of the left anterior descending artery.

Increased collagen degradation triggers progressive cardiomyocyte slippage, which leads to continued ventricular dilation. Figure 7 illustrates the progression of ventricular dilation with a maximum value of 40%. Figure 8

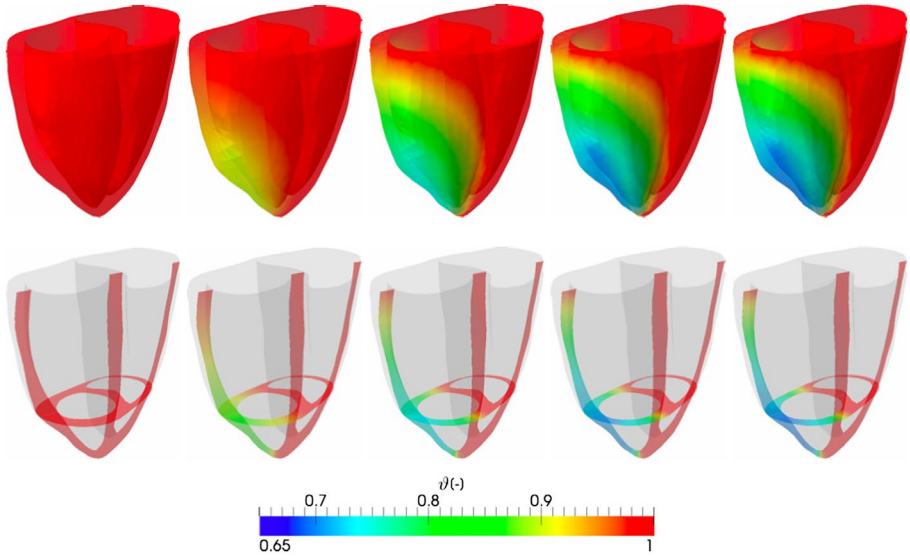

Figure 5. Evolution of the wall thinning in the left ventricle due to progressive cardiomyocyte death.

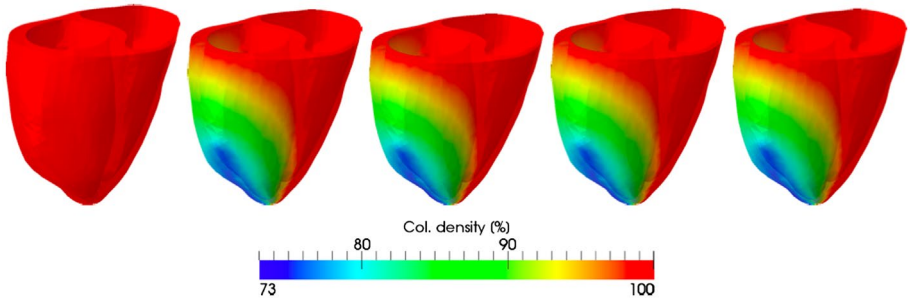

Figure 6. Evolution of collagen degradation following left anterior descending arterial occlusion.

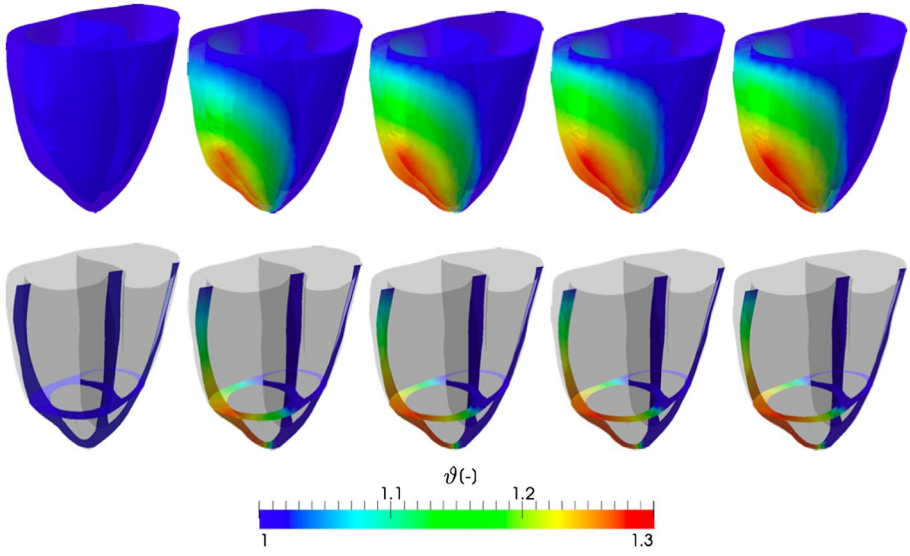

Figure 7. Evolution of ventricular dilation in response to collagen degradation.

illustrates the wall thinning and ventricular dilation in a cross sectional cut and the evolution of the ventricle thickness and the expansion area in the location of maximum ischemia.

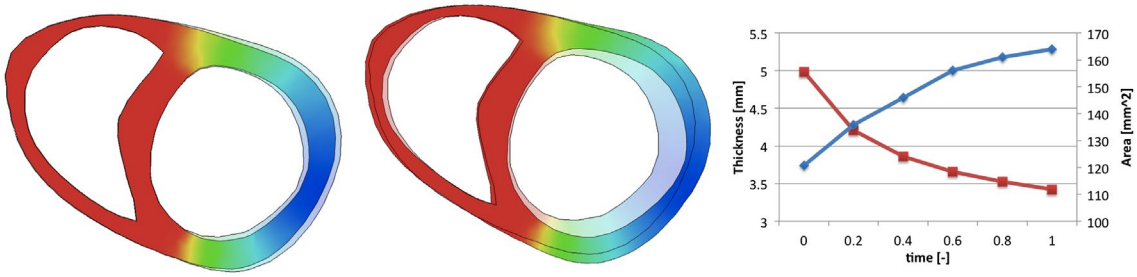

Figure 8. Wall thinning (left) and ventricular dilation (right). Translucent color shows the original geometry and solid colors show the final thinned and dilated geometry. In the right, figure displays the gradual thinning of the wall in time (red line) and the area increase of the internal ventricular surface in the region of maximum expansion (blue line).

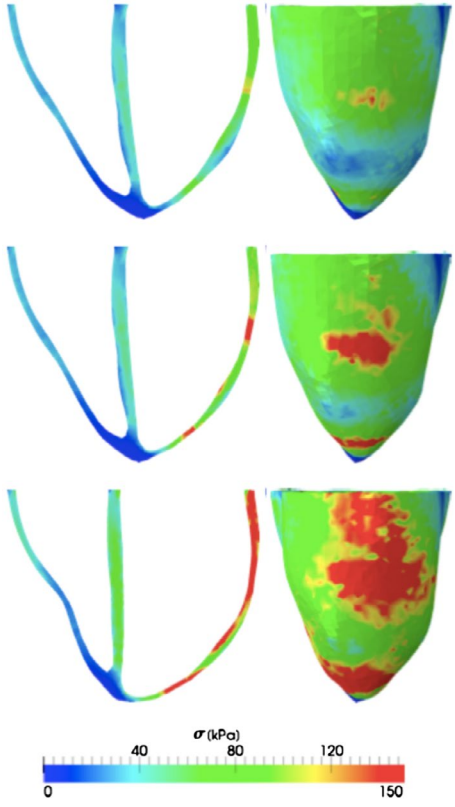

Figure 9. Spatial evolution of stresses in the healthy heart (top), after wall thinning (middle), and after ventricular dilation (bottom) at four equidistant time points across the cardiac cycle.

3.3. Mechanical model

To illustrate the effects of wall thinning and ventricular dilation, we simulate three different scenarios: a healthy heart, a wall thinned heart, and a dilated heart. To fix the heart in space, we impose Dirichlet boundary conditions in the basal plane: We fix the basal region of the septum in all three directions in space, and fix the displacements of the remaining basal regions only in the perpendicular direction. We prescribe the left and right ventricular pressures in both ventricles at the isovolumetric contraction phase according to the pressure curves in Goktepe et al. (2011).

Figure 9 summarizes the spatial evolution of the ventricular wall stresses at the beginning of the isovolumetric contraction stage (≈ 80-100kPa). In comparison to the healthy heart, top, the heart, which had undergone cardiomyocyte death and wall thinning, middle, displays a significant increase in the stress. In comparison to the healthy heart, top, the heart, which had undergone collagen degradation and ventricular dilation as can be observed in the figure, bottom, experiences a larger increase in the stress.

4. Discussion

We have introduced a new model to study the thinning and dilation of the ventricle after myocardial infarction. Previous models of cardiac growth and remodeling are driven by mechanical variables such as strain and stress (Goktepe, Abilez, & Kuhl 2010; Rausch et al. 2011). Although these rather phenomenological models compare well to clinical observations, they lack a sound biological description of the underlying biochemical phenomena in the affected tissue regions. In several pathologies, stress and strain are often viewed as triggers of cardiac remodeling (Genet et al. 2014); yet, in myocardial infarction, it is a cascade of biochemical events that initiates morphological alterations in the affected tissue regions (Cleutjens et al. 1999; Jugdutt 2003). Here we have adapted previous computational models of volumetric growth (Goktepe, Abilez, & Kuhl 2010; Sáez et al. 2014) to include biochemical effects as the driving forces for growth and remodeling. We first studied the ischemic tissue and showed how reduced oxygen supply initiates progressive cardiomyocyte death. This has, in turn, lead to thinning of the ventricular wall. At the same time, biochemical phenomena, including synthesis of matrix metalloproteinase, initiate changes in collagen content (Cleutjens et al. 1995; Jugdutt 2003). These phenomena trigger cardiomyocyte slippage and result in progressive ventricular dilation (Erlebacher et al. 1984). We have proposed evolution equations for these two cascades of events and simulated both in a finite-element setting. Our results agree well with the

clinical observations in response to myocardial infarction. Wall thinning and subsequent ventricular dilation are two well-know consequences of infarction. They are collectively referred to as short-term adaptation.

Our model has some limitations that should be mentioned. In this first step, we have neglected the electro-mechanical behavior of the heart (Baillargeon et al. 2014). We have focused exclusively on the passive material behavior. However, in our current model, growth is not driven by stress – for which we would need to account for passive and active contributions – but rather by biochemical events. Moreover, the mechanical effects of wall thinning and ventricular dilation are mainly relevant during the passive filling phase of the cycle. Nevertheless, these two effects can also affect the pump function during systole. For example, wall thinning can alter the end-diastolic strain in the ventricles and because of the Frank-Starling mechanism, this geometrical change would have an impact on the active contraction. While the contracting phase would be mainly affected by the loss of viable cardyomyocytes. This is a active mechanism of the process that we do not consider here. Therefore, we exclusively focus on the passive constitutive response. This lets us to recover some mechanical variables, including stress profiles, and allows us to directly compare alterations in response to cardiomyocyte death and collagen degradation. This model, as in many others, has a number of material parameters that are difficult to calibrate (Lee, Genet, et al. 2014).

In our future work, we would like to overcome these limitations by performing controlled experimental studies of the interaction of biochemical fields and sarcomere number on the cellular scale, cardiomyocyte density and collagen content on the tissue scale, wall thickness and chamber size on the organ scale, and ejection fraction and ventricular pressure on the system scale. We will perform a series of experiments to quantify and model the interaction of these characteristics in both space and time. We hope to create a calibrated computational model of the timeline of myocardial infarction with the ultimate goal to predict the propensity toward heart failure as a function of infarct intensity, location, and size.

Disclosure statement

No potential conflict of interest was reported by the authors.

References

Baillargeon B, Rebelo N, Fox DD, Taylor RL, Kuhl E. 2014. The living heart project: a robust and integrative simulator for human heart function. Eur J Mech A/Solids. 48:38–47.

Blankesteijn WM, Creemers E, Lutgens E, Cleutjens JP, Daemen MJ, Smits JF. 2001. Dynamics of cardiac wound healing following myocardial infarction: observations in genetically altered mice. Acta Physiol Scand. 173:75–82.

Border WA, Noble NA. 1994. Transforming growth-factor-beta in tissue fibrosis. New Engl J Med. 331:1286–1292.

Buganza Tepole A, Kuhl E. 2013. Review: systems-based approaches towards wound healing. Pediatric Res. 73: 553–563.

Buganza Tepole A, Kuhl E. 2014. Computational modeling of chemo-bio-mechanical coupling: a systems-biology approach towards wound healing. Comp Meth Biomech. Biomed Eng. doi:10.1080/10255842.2014.980821.

Buja LM, Eigenbrodt ML, Eigenbrodt EH. 1993. Apoptosis and necrosis. Basic types and mechanisms of cell death. Arch Pathol Lab Med. 117:1208–1214.

Cheng A, Nguyen TC, Malinowski M, Langer F, Liang D, Daughters GT, Ingels NB Jr, Miller DC. 2006. Passive ventricular constraint prevents transmural shear strain progression in left ventricle remodeling. Circulation. 114:I79–I86.

Cleutjens JP, Blankesteijn WM, Daemen MJ, Smits JF. 1999. The infarcted myocardium: simply dead tissue, or a lively target for therapeutic interventions. Cardiovasc Res. 44:232–241.

Cleutjens JP, Kandala JC, Guarda E, Guntaka RV, Weber KT. 1995. Regulation of collagen degradation in the rat myocardium after infarction. J Mol Cell Cardiol. 27: 1281–1292.

Eaton LW, Weiss JL, Bulkley BH, Garrison JB, Weisfeldt ML. 1979. Regional cardiac dilatation after acute myocardial infarction: recognition by two-dimensional echocardiography. N Engl J Med. 300:57–62.

Erlebacher JA, Weiss JL, Weisfeldt ML, Bulkley BH. 1984. Early dilation of the infarcted segment in acute transmural myocardial infarction: role of infarct expansion in acute left ventricular enlargement. J Am Coll Cardiol. 4:201–208.

Ertl G, Frantz S. 2005. Healing after myocardial infarction. Cardiovasc Res. 66:22–32.

Etoh T, Joffs C, Deschamps AM, Davis J, Dowdy K, Hendrick J, Baicu S, Mukherjee R, Manhaini M, Spinale FG. 2001. Myocardial and interstitial matrix metalloproteinase activity after acute myocardial infarction in pigs. Am J Physiol Heart Circ Physiol. 281:H987–H994.

Flory PJ. 1961. Thermodynamic relations for high elastic materials. T Faraday Soc. 57:829–838.

Fuster V. 1994. Lewis A. Conner memorial lecture. Mechanisms leading to myocardial infarction: insights from studies of vascular biology. Circulation. 90:2126–2146.

Genet M, Lee LC, Nguyen R, Haraldsson H, Acevedo-Bolton G, Zhang ZH, Ordovas K, Kozerke S, Guccione JM. 2014. Distribution of normal human left ventricular myofiber stress at end diastole and end systole. J Appl Phys. 117: 142–152.

Goktepe S, Abilez OJ, Kuhl E. 2010. A generic approach towards finite growth with examples of athlete's heart, cardiac dilation, and cardiac wall thickening. J Mech Phys Solids. 58:1661–1680.

Goktepe S, Abilez OJ, Parker KK, Kuhl E. 2010. A multiscale model for eccentric and concentric cardiac growth through sarcomerogenesis. J Theor Bio. 265:433–442.

Goktepe S, Acharya SNS, Wong J, Kuhl E. 2011. Computational modeling of passive myocardium. Int J Num Meth Biomed Eng. 27:1–12.

González A, Fortuño MA, Querejeta R, Ravassa S, López B, López N, Díez J. 2003. Cardiomyocyte apoptosis in hypertensive cardiomyopathy. Cardiovasc Res. 59:549–562.

Himpel G, Kuhl E, Menzel A, Steinmann P. 2005. Computational modelling of isotropic multiplicative growth. CMES. 8:119–134.

Holzapfel GA. 2000. Nonlinear solid mechanics: a continuum approach for engineering. Wiley.

Holzapfel GA, Ogden RW. 2009. Constitutive modelling of passive myocardium: a structurally based framework for material characterization. Phil Trans R Soc A. 367: 3445–3475.

Jugdutt BI. 2003. Ventricular remodeling after infarction and the extracellular collagen matrix: when is enough enough? Circulation. 108:1395–1403.

Kanduc D, Mittelman A, Serpico R, Sinigaglia E, Sinha AA, Natale C, Santacroce R, Di Corcia MG, Lucchese A, Dini L, et al. 2002. Cell death: apoptosis versus necrosis. Int J Oncol. 21:165–170.

Knowlton KU, Chien KR. 1999. Inflammatory pathways and cardiac repair: the affliction of infarction. Nat Med. 5:1122–1123.

Kumar V, Abbas AK, Aster JC. 2014. Robbins and Cotran pathologic basis of disease. Elsevier Saunders.

Lee EH. 1969. Elastic-plastic deformation at finite strains. J Appl Mech. 36:1–6.

Lee LC, Wall ST, Genet M, Hinson A, Guccione JM. 2014. Bioinjection treatment: effects of post-injection residual stress on left ventricular wall stress. J Biomech. 47:3115–3119.

Lee LC, Genet M, Dang AB, Ge L, Guccione JM, Ratcliffe MB. 2014. Applications of computational modeling in cardiac surgery. J Cardiac Surg. 29:293–302.

MacLellan WR, Schneider MD. 1997. Death by design. Programmed cell death in cardiovascular biology and disease. Circ Res. 81:137–144.

Marsden JE, Hughes TJR. 1994. Mathematical foundations of elasticity. Englewood Cliffs, New Jersey: Dover.

Menzel A, Kuhl E. 2012. Frontiers in growth and remodeling. Mech Res Comm. 42:1–14.

Olivetti G, Capasso JM, Sonnenblick EH, Anversa P. 1990. Side-to-side slippage of myocytes participates in ventricular wall remodeling acutely after myocardial infarction in rats. Circ Res. 67:23–34.

Passier R, van Laake LW, Mummery CL. 2008. Stem-cell-based therapy and lessons from the heart. Nature. 453:322–329.

Rausch MK, Dam A, Goktepe S, Abilez OJ, Kuhl E. 2011. Computational modeling of growth: systemic and pulmonary hypertension in the heart. Biomech Model Mechanobiol. 10:799–811.

Rodriguez EK, Hoger A, McCulloch AD. 1994. Stress-dependent finite growth in soft elastic tissues. J Biomech. 27:455–467.

Sáez P, Peña E, Martínez MA, Kuhl E. 2013. Mathematical modeling of collagen turnover in biological tissue. J Math Bio. 67:1765–1793.

Sáez P, Peña E, Martínez MA, Kuhl E. 2014. Computational modeling of hypertensive growth in the human carotid artery. Comput Mech. 53:1183–1196.

St. John Sutton MG, Sharpe N. 2000. Left ventricular remodeling after myocardial infarction: pathophysiology and therapy. Circulation. 101:2981–2988.

Tiyyagura SR, Pinney SP. 2006. Left ventricular remodeling after myocardial infarction: past, present, and future. Mt Sinai J Med. 73:840–851.

Visse R, Nagase H. 2003. Matrix metalloproteinases and tissue inhibitors of metalloproteinases – structure, function, and biochemistry. Circ Res. 92:827–839.